Contents

List of Figures

List of Tables

Experimental Section

Materials and sample preparation

^{F}rG and ^{F}araG modified oligonucleotides were purchased from IBA (Göttingen, Germany) and quantified based on their absorbance at 260 nm after ethanol precipitation. NMR samples were prepared by dialyzing the corresponding oligonucleotide against 10 mM potassium phosphate buffer at pH 7, followed by heating to 90 °C for 5 min and subsequent cooling to room temperature. Concentrations of NMR samples were about 0.4 mM. For optical measurements, oligonucleotide concentrations of 5 µM were used in a buffer containing 20 mM potassium phosphate, 100 mM KCl, pH 7.

Optical measurements

Circular dichroism (CD) spectra were acquired with 5 accumulations, a scanning speed of 50 nm/min and a bandwidth of 1 nm at 25 °C on a Jasco J-810 spectropolarimeter (Jasco, Tokyo, Japan). All spectra were blank-corrected by subtraction of the buffer spectrum. Melting curves were recorded in triplicate on a Jasco V-650 spectrophotometer equipped with a Peltier temperature control unit (Jasco, Tokyo, Japan) with quartz cuvettes of 10 mm path length. The absorbance at 295 nm was measured between 10 and 90 °C in 0.5 °C intervals with a heating rate of 0.2 °C/min. The melting point T_m was determined from the minimum of the first derivative of the heating phase.

NMR spectroscopy

All NMR spectra were acquired on a Bruker Avance Neo 600 MHz spectrometer equipped with an inverse ^{1}H/^{13}C/^{15}N/^{19}F quadruple resonance cryoprobehead and z-field gradients. For spectral processing and analysis, Topspin 4.0.4 and CcpNmr Analysis 2.4 were employed.[1] Spectra were acquired at 25 °C in 10 mM KP_i buffer using the water resonance for ^{1}H referencing. An optimized WATERGATE[2] with w5 element was employed for solvent suppression in 1D spectra and 2D NOE experiments. NOESY spectra were recorded with mixing times of 80–300 ms in either 90 % H_2O/10 % D_2O or 100 % D_2O with or without broadband ^{19}F decoupling using the waltz16 sequence. DQF-COSY spectra were acquired in D_2O with solvent suppression through presaturation. Phase-sensitive ^{1}H-^{13}C HSQC experiments optimized for a $^{1}J_{CH}$ of 170 Hz were acquired with a 3-9-19 solvent suppression scheme in 90 % H_2O/10 % D_2O usually employing a spectral width of 7.5 kHz in the indirect ^{13}C dimension and 512 t_1 increments. ^{13}C chemical shifts were referenced relative to DSS using the indirect referencing method. ^{19}F spectra were acquired without and with broadband ^{1}H decoupling using the waltz16 sequence. 2D ^{19}F-^{1}H HOESY spectra with a 350 ms mixing time were acquired with a spectral width of 2.4 kHz in the indirect ^{1}H dimension and 240 t_1 increments. ^{19}F chemical shifts were referenced relative to TFA using the indirect referencing method (factor 0.940867).[3]

NMR structure calculations

A simulated annealing protocol in Xplor-NIH 2.49 was used to generate 100 starting structures of the DNA sequence.[4] The RED software was used to calculate the partial atomic charges for the modified ^{F}rG and ^{F}araG residues for subsequent calculations with Amber16.[5,6] A restrained simulated annealing was performed in implicit water using the parmbsc0 force field including the χ_{OL4}, $\varepsilon\xi_{OL1}$, and β_{OL1} corrections.[7–10]

2D NOE crosspeaks were classified as strong (2.9 ± 1.1 Å), medium (4.0 ± 1.5 Å), weak (5.5 ± 1.5 Å), or very weak (6.0 ± 1.5 Å). For exchangeable protons, categories were set to medium (4.0 ± 1.2 Å), weak (5.0 ± 1.2 Å), or very weak (6.0 ± 1.2 Å). In case of strongly overlapped signals, distances were set to 5.0 ± 2.0 Å. Glycosidic torsions were restrained in the range 170–310° or 25–95° for *anti* and *syn* conformers, respectively. The pseudorotation phase angle (PPA) was restricted to 144–180° for experimentally determined (based on DQF-COSY spectra) *south*-type conformers (all DNA residues except for residues A9-A13 in A14F15 and G2, A9, C12, and A13 in F14A15). The G analogs in A14F15 were restrained to a sugar pucker in the *north* domain with the usual PPA range of 0–90° for ^{F}araG14 and a narrower range of 35–90° for ^{F}rG15. The latter restraint was based on the estimation of the PPA to 50–70° by a comparison of experimentally determined $^{3}J_{F2'H1'}$ and $^{3}J_{F2'H3'}$ (Tab. S2) with values predicted using a Karplus-type relationship between vicinal ^{1}H-^{19}F coupling constants and H-C-C-F torsion angles.[11] Using the same relation, the PPA of ^{F}rG14 in F14A15 was restrained in the range 120–180°, while the usual *south*-type restraint was used for ^{F}araG15. For F14A15, the C12-A13 O2···H-N6 hydrogen bond, which was found in the majority of states in the early stage of structure calculation, was also restrained for subsequent simulated annealing iterations based on the observation of two distinct amino signals for A13 and NOE crosspeaks of A13 H62 to imino protons of the bottom tetrad (Fig. S9).

For a simulated annealing of the 100 starting structures, a 5 ps equilibration period at 300 K was followed by heating to 1000 K during 10 ps. After 30 ps, the system was cooled to 100 K and finally to 0 K within 45 ps and 10 ps, respectively. Force constants for NMR-derived distance restraints were set to 40 kcal·mol^{-1}·Å^{-2}, for hydrogen bond restraints

to 50 kcal·mol^{-1}·Å^{-2}, for glycosidic torsion angle and sugar pucker restraints to 200 kcal·mol^{-1}·rad^{-2}, and for planarity restraints of G-tetrads to 30 kcal·mol^{-1}·Å^{-2}.

For a refinement in water, ten lowest energy structures were neutralized with K^+ ions and two of the cations placed in the center between the eight O6 atoms of two adjacent tetrads. The system was hydrated with TIP3P water molecules in a truncated octahedral box of 10 Å.[12] During initial equilibration, the DNA was fixed with 25 kcal·mol^{-1}·Å^{-2}. After 500 steps of steepest descent and conjugate gradient minimization, the system was heated from 100 to 300 K during 10 ps under constant volume, followed by a decrease in force constants to 5, 4, 3, 2, 1 and 0.5 kcal·mol^{-1}·Å^{-2} and further equilibration. The final simulation of 4 ns duration at 1 atm was performed with restraints only for NMR-derived distances and Hoogsteen hydrogen bonds. The trajectories were subsequently averaged over the last 500 ps and shortly minimized in vacuum for 500 steps. Atomic coordinates of an ensemble of ten final structures with the lowest energy have been deposited in the Protein Data Bank (accession code 6TC8 for A14F15 and 6TCG for F14A15). Structural parameters were determined with the 3DNA software package.[13]

Resonance Assignment

A14F15

Based on identical topologies for A14F15 and the recently reported F(14,15) quadruplex,[14] resonance assignment of the majority of non-exchangeable protons was easily accomplished through uninterrupted sequential NOE contacts within G-tracts both in the H8-H2'/H2" and H8-H1' region (Fig. S1). ^{F}rG15 and G16 are connected by an unusual reversed sequential contact between ^{F}rG15 H8 and G16 H1' as in F(14,15) and the corresponding rG modified structural analog.[14] G1, G6, and G20 as well as ^{F}araG14 show strong intraresidual H8-H1' NOE crosspeaks as well as characteristically downfield shifted ^{13}C8 resonances (Fig. S3) in agreement with their expected *syn* conformation. Sequential NOE contacts extending into loop regions allowed for the assignment of the G3-A4-T5 lateral loop (Fig. S1), as well as of the A18-C19 propeller loop (not shown). While A9 and A11 could not be assigned, the assignment of C10, C12, and A13 was possible based on a comparison with F(14,15) (Fig. S4). The A13 assignment was further confirmed through two NOE contacts to imino protons of the bottom tetrad (Fig. S2). The twelve well resolved imino proton resonances were unambiguously assigned through a nearly complete set of intra-tetrad H1-H8 NOE contacts, which are in perfect agreement with the expected hydrogen bonding pattern (Fig. S2). D_2O/H_2O exchange confirmed the assignment of central tetrad imino resonances with reduced intensities for G1, G7, G16, and G21 shortly after addition of H_2O (Fig. S5). Finally, H1-H1 contacts between and within G-tracts clearly show the heteropolar and homopolar stacking of top and bottom tetrad onto the central G-quartet, respectively (Fig. S2). ^{19}F2' resonances of G analogs were assigned from intraresidual contacts to sugar and base protons in a ^{19}F-^{1}H HOESY experiment (Fig. S6).

F14A15

For F14A15, the presence of only three *syn* Gs as identified from the characteristically strong H8-H1' NOE contacts (Fig. S7) and from unusually downfield shifted ^{13}C8 resonances (Fig. S8) proves incompatible with the structure of F(14,15) with its four Gs in the *syn* conformation. Instead, uninterrupted sequential NOE connectivities can be traced along three all-*anti* G-tracts. The G6-G7-G8 tract was easily identified by uninterrupted sequential contacts to the preceding G3-A4-T5 segment. The assignment of the ^{F}araG15-G16-G17 tract was equally straightforward due to the characteristic 50 Hz splitting of the ^{F}araG15 H2' resonance. The remaining all-*anti* tract could only belong to G20-G21-G22, as already assigned G3 does not exhibit any contact to other G residues, precluding a G1-G2-G3 tract. The only remaining unassigned guanosine residues, G1, G2, and ^{F}rG14 were thus identified as the three *syn* Gs of the structure.

Partially broken sequential connectivities extend into all loops, confirming the G-tract assignment and enabling the assignment of all loop residues. Thus, A9 is identified by a complete set of sequential contacts to G8. A18 H8 has a contact to G17 H1', and C19 H6 exhibits an NOE crosspeak to A18 H2'. Similarly, both A13 and A11 H8 resonances show NOE contacts to H2' resonances of their 5'-neighboring cytidine residues and were later distinguished by NOE contacts of A13 H8 and H2 to ^{F}rG14 H1 (see below).

Imino resonances were assigned based on strong intra-tetrad H1-H8 NOE contacts, assuming the same topology as F(14,15) but with a reversed top tetrad (Fig. 1D). This assumption was based on the presence of three all-*anti* G-tracts together with the three *syn* Gs. For the latter, participation in an all-*syn* G-tract as residual column of the G-core is in agreement with the absence of any sequential connectivities to either of the *syn* Gs as expected for *syn-syn* steps. H1 resonances of G20, G21, and G22 were thus easily identified through contacts with H8 of G6, G7, and G8 (Fig. S9). Likewise, ^{F}araG15, G16, and G17 H1 resonances were assigned through their NOE crosspeaks to G20, G21, and G22 H8. Additional inter-tetrad H8-H1 contacts and H1-H1 contacts within the G-tracts are in full agreement with these assignments. H8-H1 contacts between the ^{F}araG15-G16-G17 tract and the G2-G1-^{F}rG14 column are incomplete, yet imino resonances of G1 and G2 can be identified through an additional inter-tetrad H1-H8 crosspeak between G1 and ^{F}araG15. The imino resonance of ^{F}rG14 was then assigned based on complete H1-H1 contacts within this G-tract and confirmed through contacts to aromatic protons of 5'-neighboring A13.

The identification of imino resonances of the central tetrad through D_2O/H_2O exchange (Fig. S5) further confirmed G1, G16, and G21 H1 assignments and supported the assignment of the remaining set of H1-H1 contacts and the still unassigned non-exchangeable protons of the three *syn* Gs. The remaining imino resonance of the central tetrad was thus identified as G7 H1 and its NOE contact to the H8 resonance at 7.18 ppm allowed for the assignment of the latter to G1. Consequently, the other two *syn* Gs, G2 and ^{F}rG14, were assigned to the H8 resonances at 7.75 ppm and 6.82 ppm, respectively. The latter is unambiguously traced to ^{F}rG14 because of the splitting of its H2' resonance scalar coupled to F2' (Fig. 3C). G6 H1 was subsequently identified through its NOE crosspeak to G2 H8. In spite of a missing H1-H8 contact with ^{F}rG14, G8 H1 was assigned through its NOE contact with G7 H1. The assignment of both G8 and G7 imino resonances is confirmed through weak inter-tetrad NOE contacts with H8 resonances of G1 and G2, and additional support for G1 and G2 assignments comes from sequential contacts between G2 H1 and H2'/H2" of G1. ^{19}F2' resonances of G analogs were assigned from intraresidual F2'-H2' contacts in a ^{19}F-^{1}H HOESY experiment (Fig. S10).

References

[1] W. F. Vranken, W. Boucher, T. J. Stevens, R. H. Fogh, A. Pajon, M. Llinas, E. L. Ulrich, J. L. Markley, J. Ionides and E. D. Laue, *Proteins Struct. Funct. Genet.*, 2005, **59**, 687–696.

[2] J. Wang, X. Zhang, P. Sun, X. Jiang, B. Jiang, C. Cao and M. Liu, *J. Magn. Reson.*, 2010, **206**, 205–209.

[3] T. Maurer and H. R. Kalbitzer, *J. Magn. Reson. Ser. B*, 1996, **113**, 177–178.

[4] C. D. Schwieters, J. J. Kuszewski, N. Tjandra and G. M. Clore, *J. Magn. Reson.*, 2003, **160**, 65–73.

[5] E. Vanquelef, S. Simon, G. Marquant, E. Garcia, G. Klimerak, J. C. Delepine, P. Cieplak and F. Y. Dupradeau, *Nucleic Acids Res.*, 2011, **39**, W511–W517.

[6] D. Case, D. Cerutti, T. Cheatham, III, T. Darden, R. Duke, T. Giese, H. Gohlke, A. Goetz, D. Greene, N. Homeyer, S. Izadi, A. Kovalenko, T. Lee, S. LeGrand, P. Li, C. Lin, J. Liu, T. Luchko, R. Luo, D. Mermelstein, K. Merz, G. Monard, H. Nguyen, I. Omelyan, A. Onufriev, F. Pan, D. York and P. Kollman, *Univ. California, San Francisco*, 2016.

[7] C. I. Bayly, K. M. Merz, D. M. Ferguson, W. D. Cornell, T. Fox, J. W. Caldwell, P. A. Kollman, P. Cieplak, I. R. Gould and D. C. Spellmeyer, *J. Am. Chem. Soc.*, 1995, **117**, 5179–5197.

[8] M. Zgarbová, M. Otyepka, J. Šponer, A. Mládek, P. Banáš, T. E. Cheatham and P. Jurečka, *J. Chem. Theory Comput.*, 2011, **7**, 2886–2902.

[9] M. Krepl, M. Zgarbová, P. Stadlbauer, M. Otyepka, P. Banáš, J. Koča, T. E. Cheatham, P. Jurečka and J. Šponer, *J. Chem. Theory Comput.*, 2012, **8**, 2506–2520.

[10] M. Zgarbová, J. Šponer, M. Otyepka, T. E. Cheatham, R. Galindo-Murillo and P. Jurečka, *J. Chem. Theory Comput.*, 2015, **11**, 5723–5736.

[11] C. Thibaudeau, J. Plavec and J. Chattopadhyaya, *J. Org. Chem.*, 1998, **63**, 4967–4984.

[12] W. L. Jorgensen, J. Chandrasekhar, J. D. Madura, R. W. Impey and M. L. Klein, *J. Chem. Phys.*, 1983, **79**, 926–935.

[13] X. J. Lu and W. K. Olson, *Nucleic Acids Res.*, 2003, **31**, 5108–5121.

[14] L. Haase, J. Dickerhoff and K. Weisz, *Chem. Eur. J.*, 2020, **26**, 524–533.

Supplementary Figures

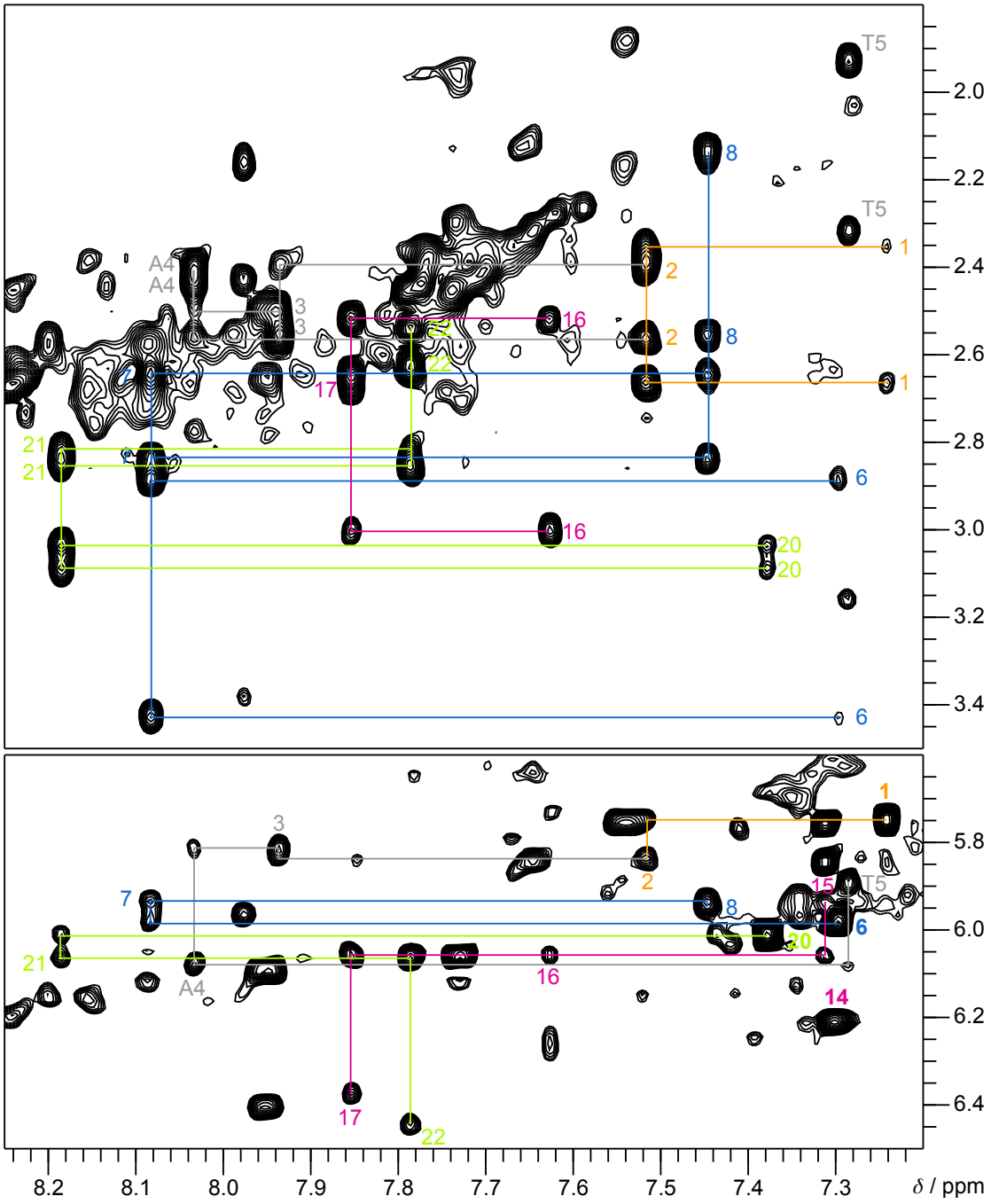

Fig. S1 Portions of a 2D NOE spectrum of A14F15 (0.4 mM) acquired at 25 °C in 10 mM KP_i, pH 7. Sequential contacts are traced in different colors for the four G-tracts in the aromatic-H2'/H2" (top) and the aromatic-H1' region (bottom). Contacts extending into loop regions are traced and labeled in grey. Strong H8-H1' crosspeaks for *syn* residues are highlighted in bold.

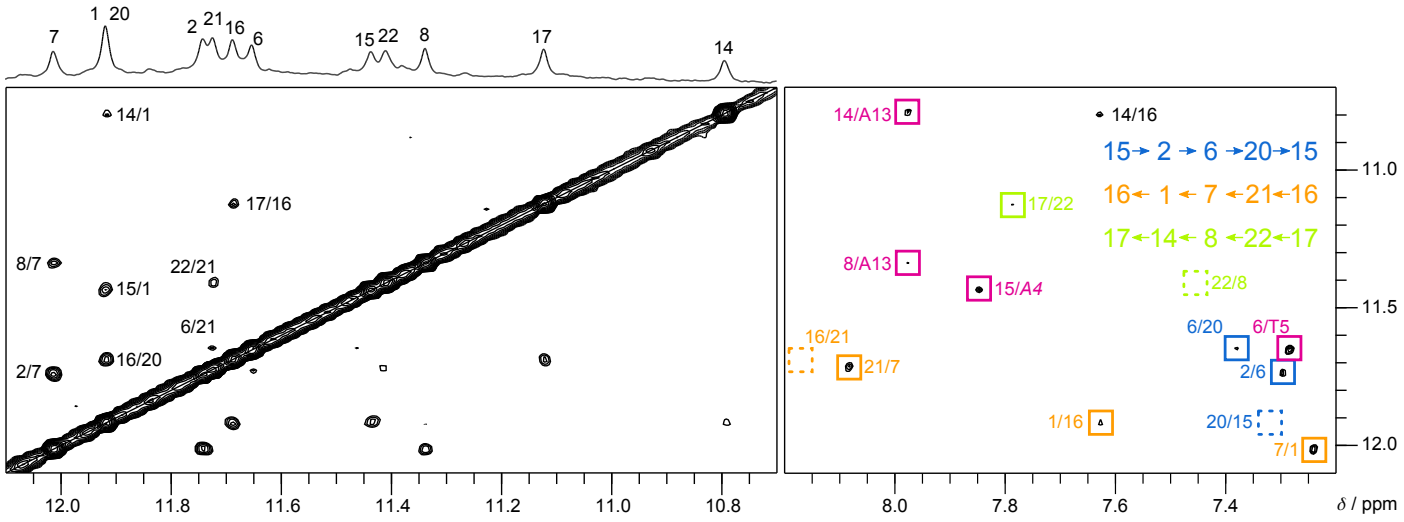

Fig. S2 Portions of a 2D NOE spectrum of A14F15 (0.4 mM) acquired at 25 °C in 10 mM KP_i, pH 7, showing H1(ω_1)-H1(ω_2) (left) and H1(ω_1)-H8(ω_2) contacts (right) framed in blue, orange, and green for top, central, and bottom tetrad, respectively. The resulting hydrogen bond directionality is indicated by arrows. The presence of weak contacts not visible at the displayed contour level is indicated by dashed squares. Contacts of outer tetrad imino resonances to loop residues are framed in magenta. Adenosine H2 resonances are labeled in italic.

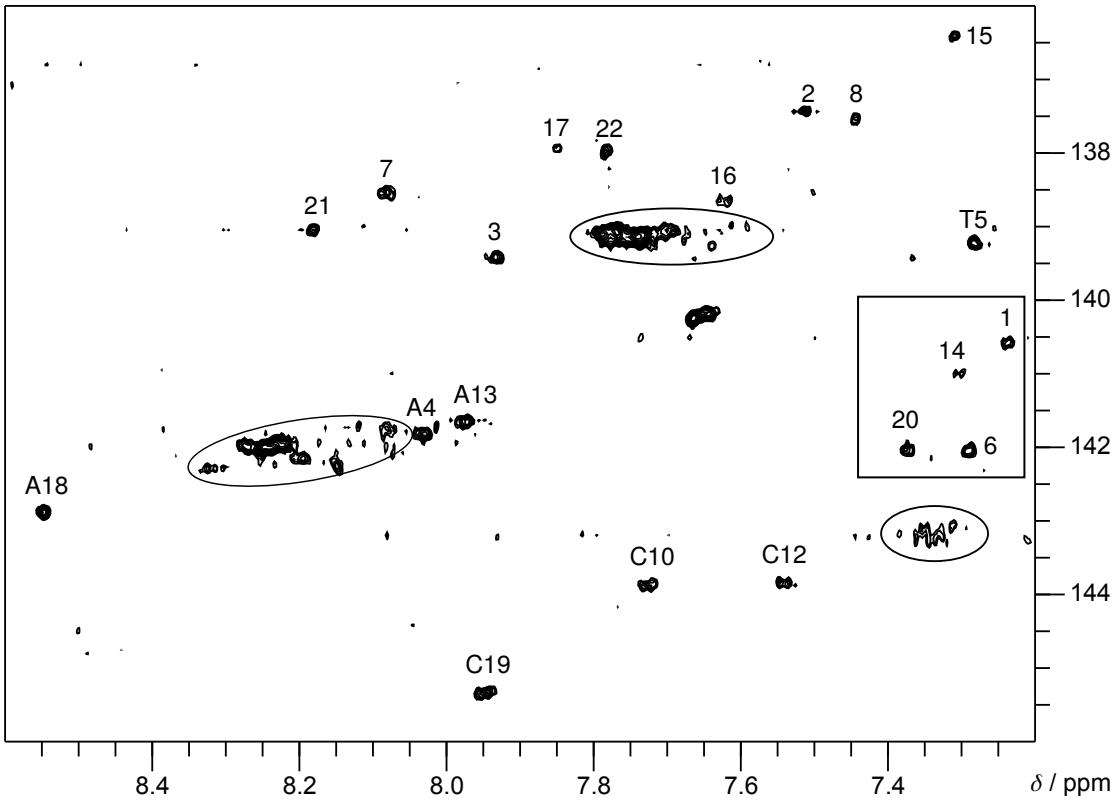

Fig. S3 H6/8-C6/8 region from a ^{1}H-^{13}C HSQC spectrum of A14F15 (0.4 mM) acquired at 25 °C in 10 mM KP_i, pH 7. *Syn* guanosines including ^{F}araG14 and signals arising from unfolded or minor species are framed by rectangles and ellipses, respectively.

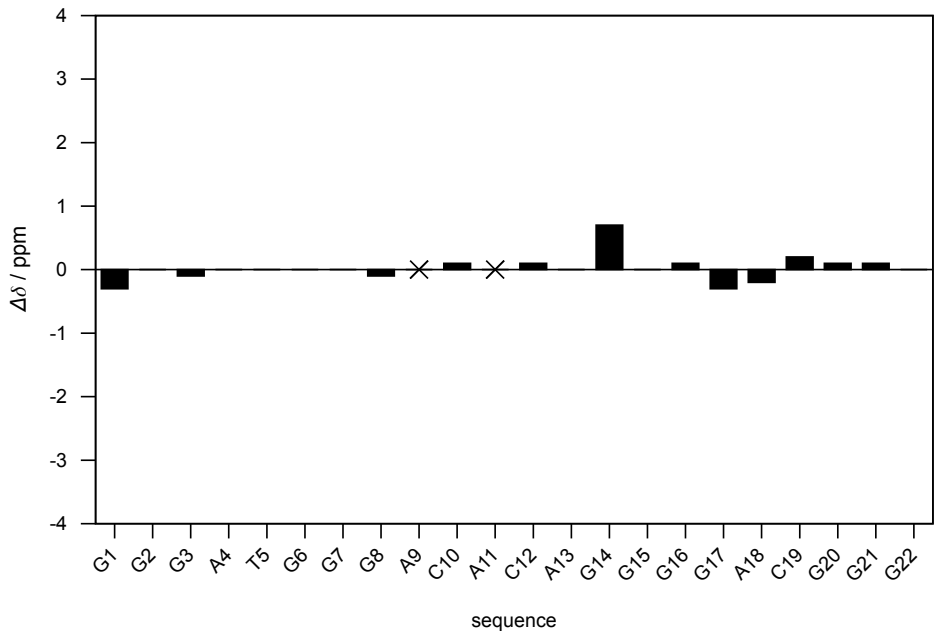

Fig. S4 Residue-wise differences in ^{13}C6/8 chemical shifts ($\Delta\delta$) between A14F15 at 25 °C and F(14,15) at 40 °C. The temperature difference for the two data sets cannot be avoided as spectral quality is considerably reduced for A14F15 at higher temperatures due to the increasing presence of single strand resonances, whereas ^{F}rG14 resonances in F(14,15) were broadened beyond detection at lower temperatures.[14] Crosses indicate residues with unassigned ^{13}C6/8 resonances. Folding into the same structure is indicated by small $\Delta\delta$ values with changes of more than 0.5 ppm only observed for position 14 carrying a different type of modification in the two sequences.

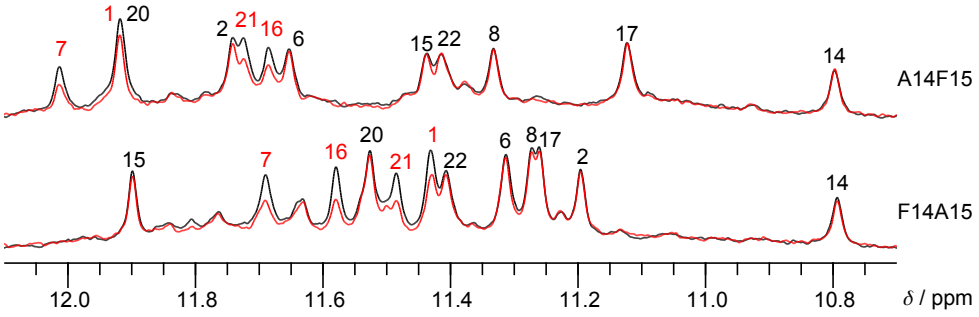

Fig. S5 D_2O/H_2O exchange experiments for A14F15 (top) and F14A15 (bottom). Imino proton region of spectra recorded 10 min (colored) and 30 min (in black) after drying and redissolving a D_2O sample in H_2O. Imino protons of the central tetrad (labelled in color) are protected from fast solvent exchange and thus identified by their reduced intensities shortly after H_2O addition.

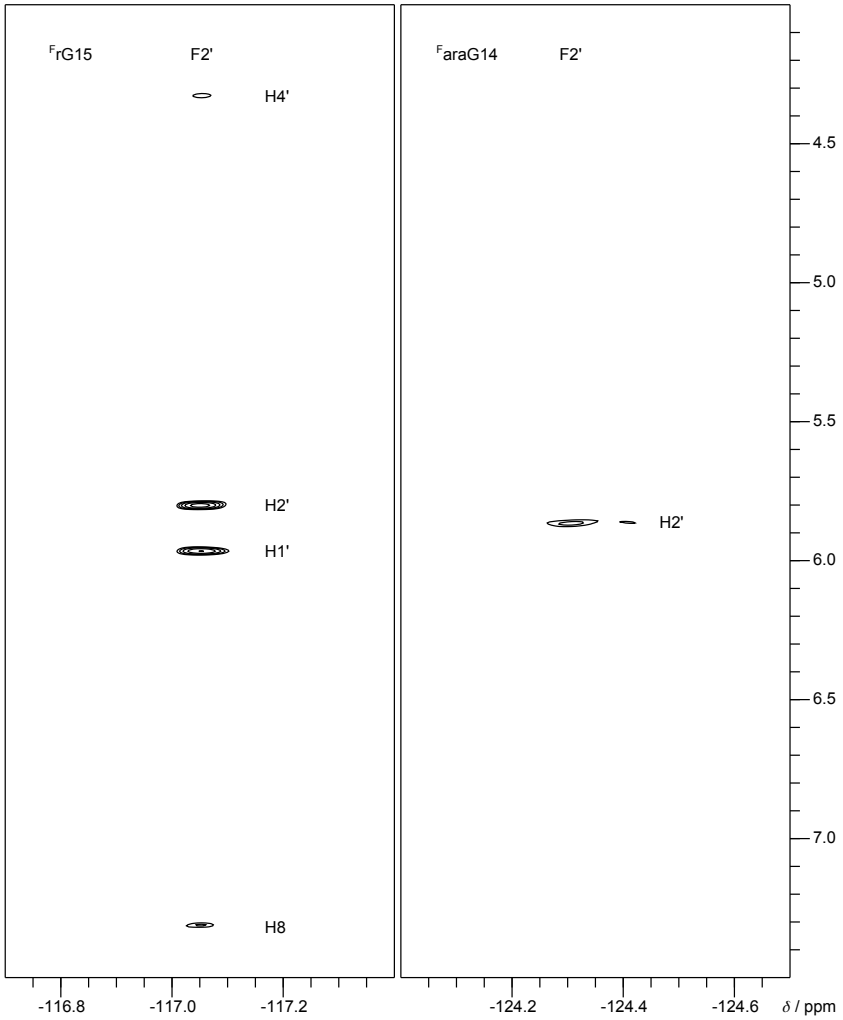

Fig. S6 Portions of a ^{19}F-^{1}H HOESY spectrum (mixing time 350 ms) of A14F15 (0.4 mM) acquired at 25 °C in 10 mM KP_i, pH 7, showing intraresidual F2'(ω_2)-H(ω_1) contacts for ^{F}rG15 (left) and ^{F}araG14 (right).

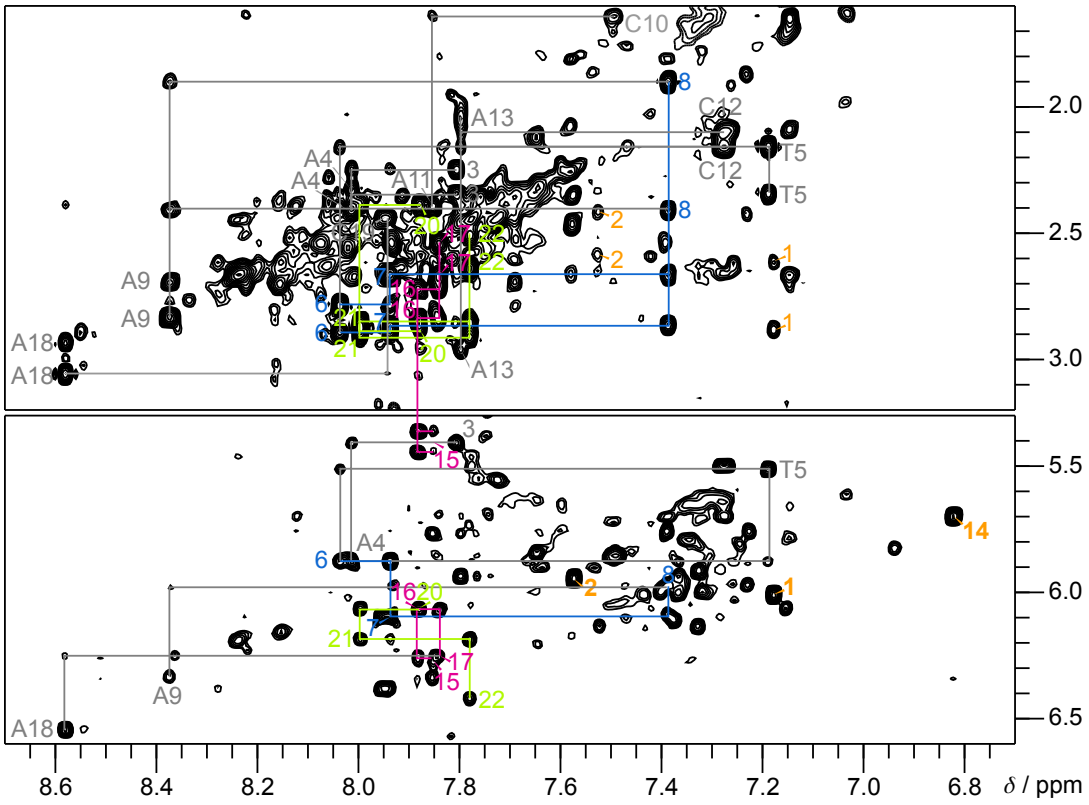

Fig. S7 Portions of a 2D NOE spectrum of F14A15 (0.4 mM) acquired at 25 °C in 10 mM KP_i, pH 7. Sequential contacts are traced in different colors for the four G-tracts in the aromatic-H2'/H2" (top) and the aromatic-H1' region (bottom). Contacts extending into loop regions are traced and labeled in grey. Strong H8-H1' crosspeaks for *syn* residues are highlighted in bold.

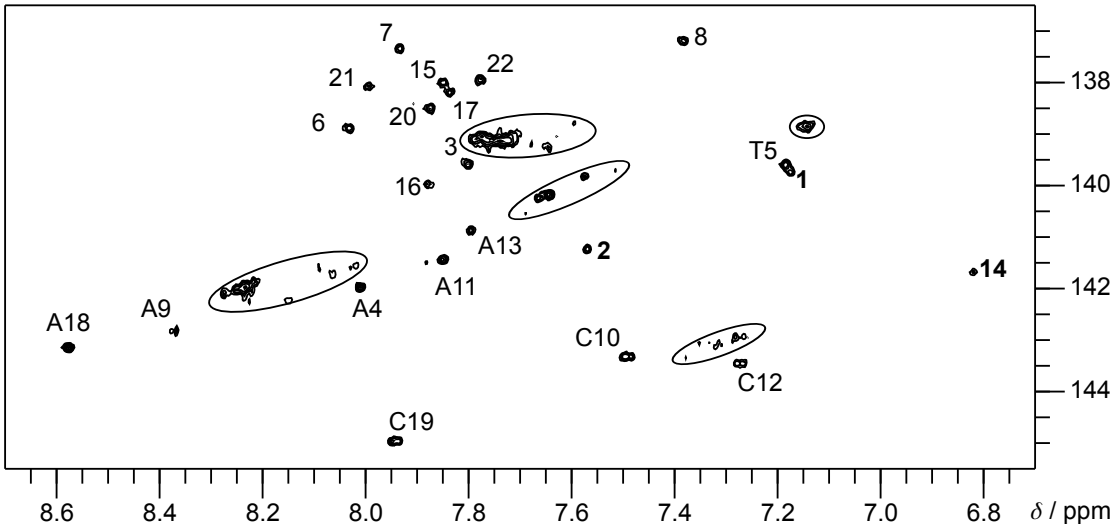

Fig. S8 H6/8-C6/8 region from a ^{1}H-^{13}C HSQC spectrum of F14A15 (0.4 mM) acquired at 25 °C in 10 mM KP_i, pH 7. Regions with signals arising from unfolded or minor species are encircled and *syn* guanosines including ^{F}rG14 are highlighted in bold.

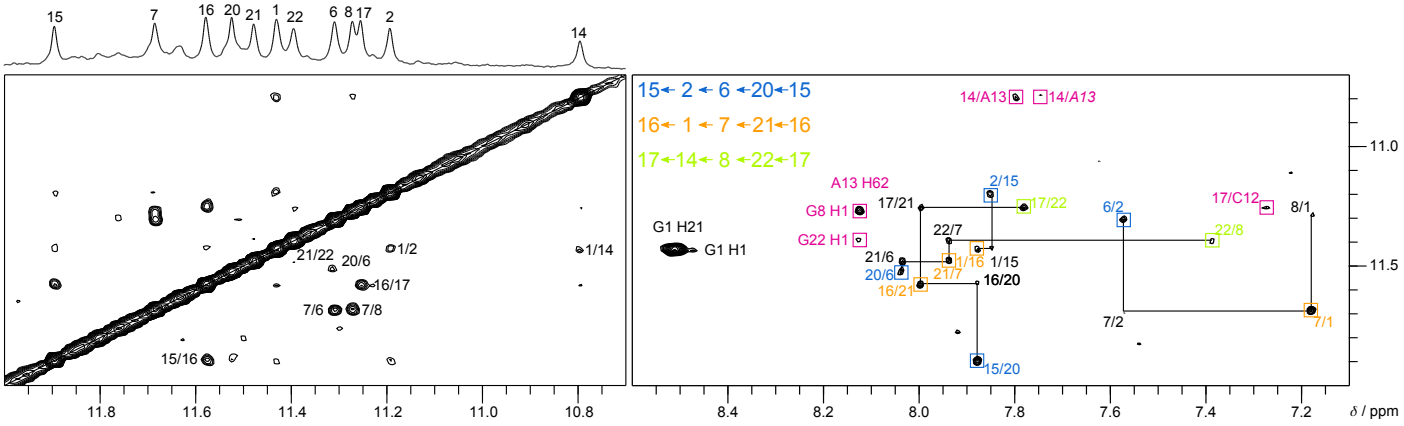

Fig. S9 Portions of a 2D NOE spectrum of F14A15 (0.4 mM) acquired at 25 °C in 10 mM KP_i, pH 7, showing H1(ω_1)-H1(ω_2) contacts (left) and imino contacts to aromatic and amino protons (right). Intra-tetrad H1(ω_1)-H8(ω_2) contacts (framed in blue, orange, and green for top, central, and bottom tetrad, respectively) determine the hydrogen bond directionality within tetrads as indicated by arrows. Additional inter-tetrad H1(ω_1)-H8(ω_2) contacts are labeled and traced with horizontal and vertical lines. Contacts of outer tetrad imino resonances to aromatic protons of C12 and A13 (H2 in italic) as well as an amino proton of A13 are framed in magenta. Presence of the latter contact points to involvement of this amino proton in hydrogen bonding.

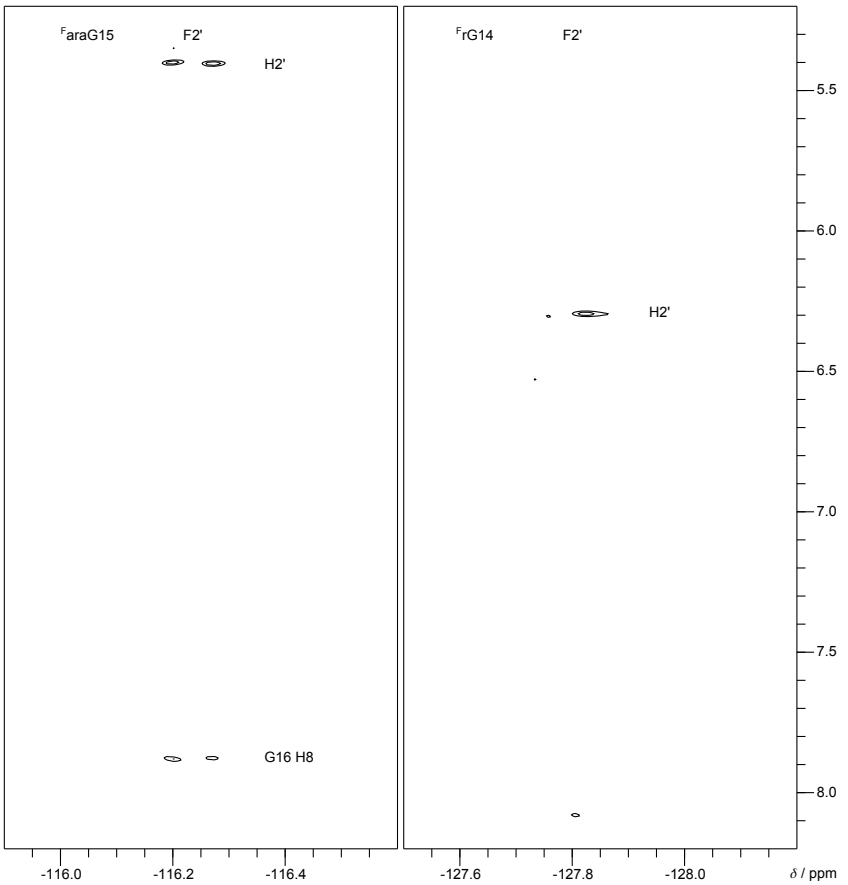

Fig. S10 Portions of a ^{19}F-^{1}H HOESY spectrum (mixing time 350 ms) of F14A15 (0.4 mM) acquired at 25 °C in 10 mM KP_i, pH 7, showing intraresidual F2'(ω_2)-H2'(ω_1) contacts for ^{F}araG15 (left) and ^{F}rG14 (right). The additional sequential contact between ^{F}araG15 F2' and G16H8 is in agreement with an observed F2'···H8-C8 hydrogen bond between these two residues (Fig. 3B).

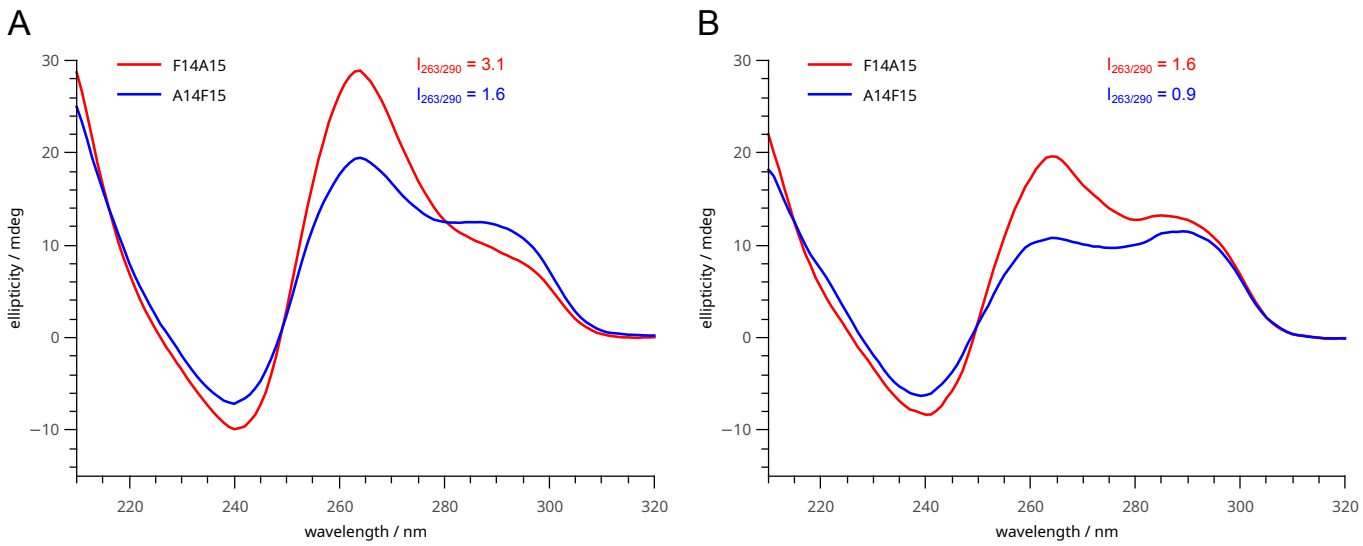

Fig. S11 CD spectra of A14F15 (blue) and F14A15 (red) acquired at 25 °C on the G4 (5 µM) in 20 mM KP_i buffer, 100 mM KCl, pH 7 (A) and in 10 mM KP_i buffer, pH 7 (B). A) With one negative signal at 240 nm and two positive bands at 263 and 290 nm, A14F15 exhibits the typical CD signature of a hybrid-type quadruplex with both homopolar and heteropolar stacking interactions between tetrads. For F14A15, ellipticity at 290 nm is reduced in agreement with exclusively homopolar G-quartet stacking. A noticeable shoulder at 290 nm may arise from additional stacking interactions of the C12-A13 base pair (Fig. S14 A) and/or from minor species as also indicated by weak signals in the imino region of the ^{1}H NMR spectrum (Fig. 2). B) In 10 mM KP_i, the ratio of CD amplitudes at 263 and 290 nm ($I_{263/290}$) is reduced by a factor of 1.8-1.9 for both A14F15 and F14A15. Although the F14A15 quadruplex shows significant intensity at 290 nm in 10 mM KP_i, its $I_{263/290}$ ratio is nearly twice as high compared to A14F15 under both buffer conditions in line with more homopolar vs. heteropolar stacking interactions.

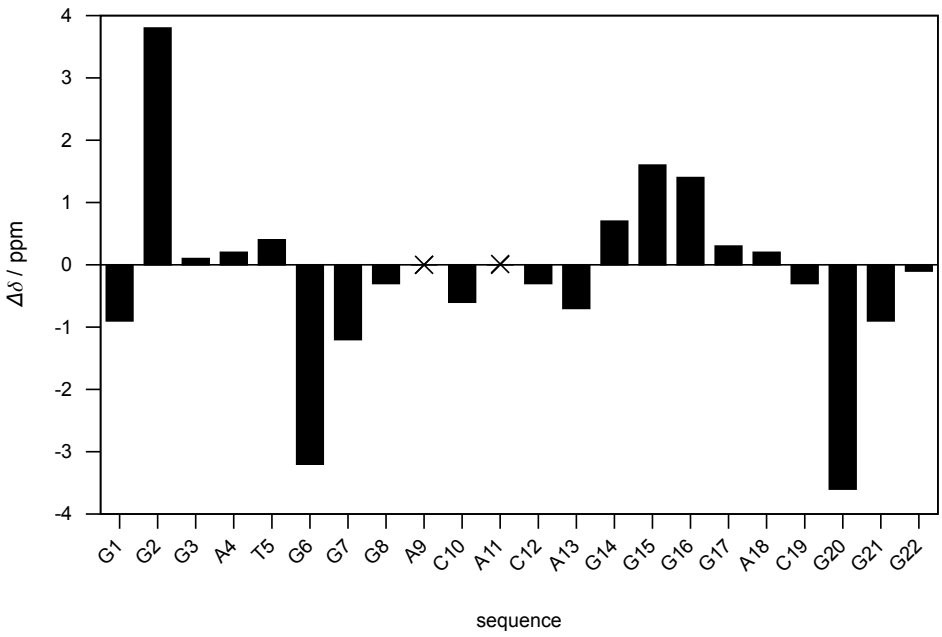

Fig. S12 Differences in ^{13}C6/8 chemical shifts ($\Delta\delta$) between F14A15 and A14F15 at 25 °C. Crosses indicate residues without assigned ^{13}C6/8 resonances. A downfield shift for G2 along with upfield shifts for G6 and G20, all in the range 3-4 ppm, indicates a concerted rotation about the glycosidic bond angle for these three residues of the top G-quartet accompanied by a tetrad polarity reversal. A small $\Delta\delta$ for residue 15, adopting an *anti* conformation in both structures, may be explained by the different type of G analog and the distinct V-loop conformations. The downfield shift of G16 ^{13}C8 may be attributed to its deshielding due to participation in a sequential hydrogen bond with ^{F}araG15 F2' (Fig. 5A).

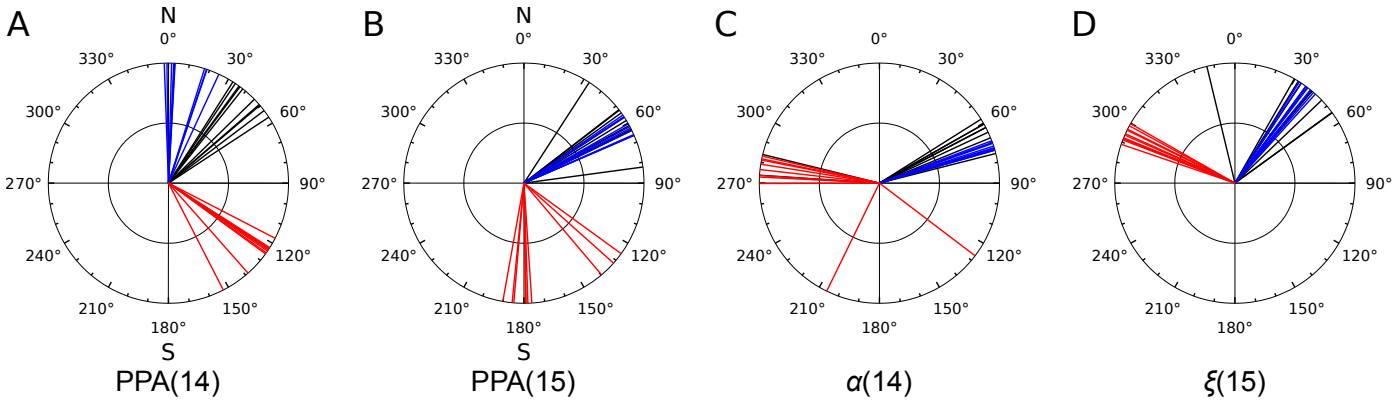

Fig. S13 V-loop conformational parameters of modified residues 14 and 15 as derived from ten low-energy structures of F(14,15) (PDB ID 6RS3, in black), A14F15 (in blue), and F14A15 (in red). The distinct V-loop conformation of F14A15 when compared to F(14,15) and A14F15 is not only expressed in differences for the pseudorotation phase angle of residue 14 (A) and 15 (B) but also for the backbone torsion angle α of residue 14 (C) and ζ of residue 15 (D).

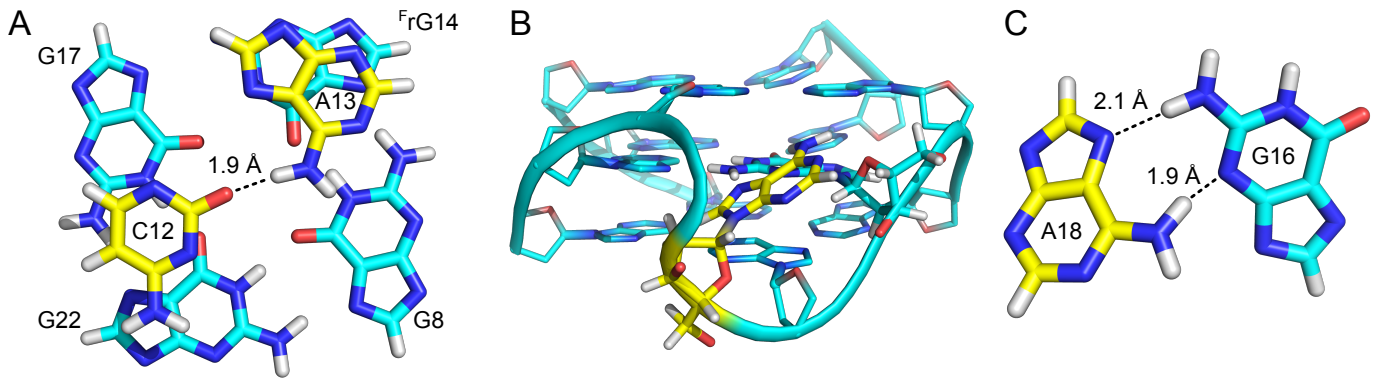

Fig. S14 Interactions of loop residues in F14A15. (A) Stacking of the C12-A13 base pair onto the bottom tetrad. (B) A18 interaction with the central tetrad. (C) Close-up view onto residues G16 and A18 interacting through two potential hydrogen bonds.

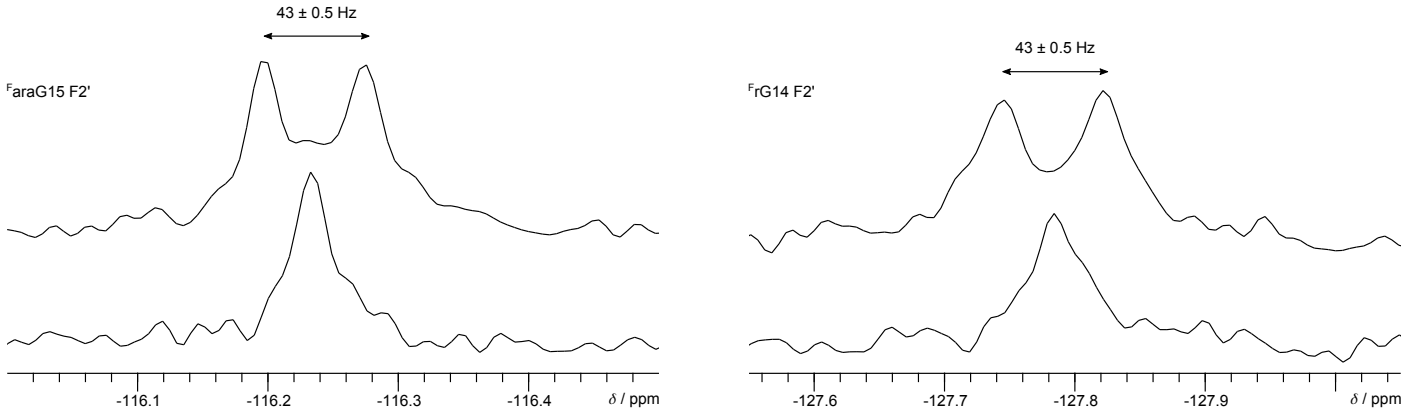

Fig. S15 Broadband ^{1}H decoupled ^{19}F spectra of F14A15 with (bottom) and without (top) homonuclear decoupling. The 43 Hz splitting of the two ^{19}F2' resonances arises from through-space scalar coupling as explained by short F2'-F2' distances around 2.8 Å seen in the high-resolution structural ensemble.

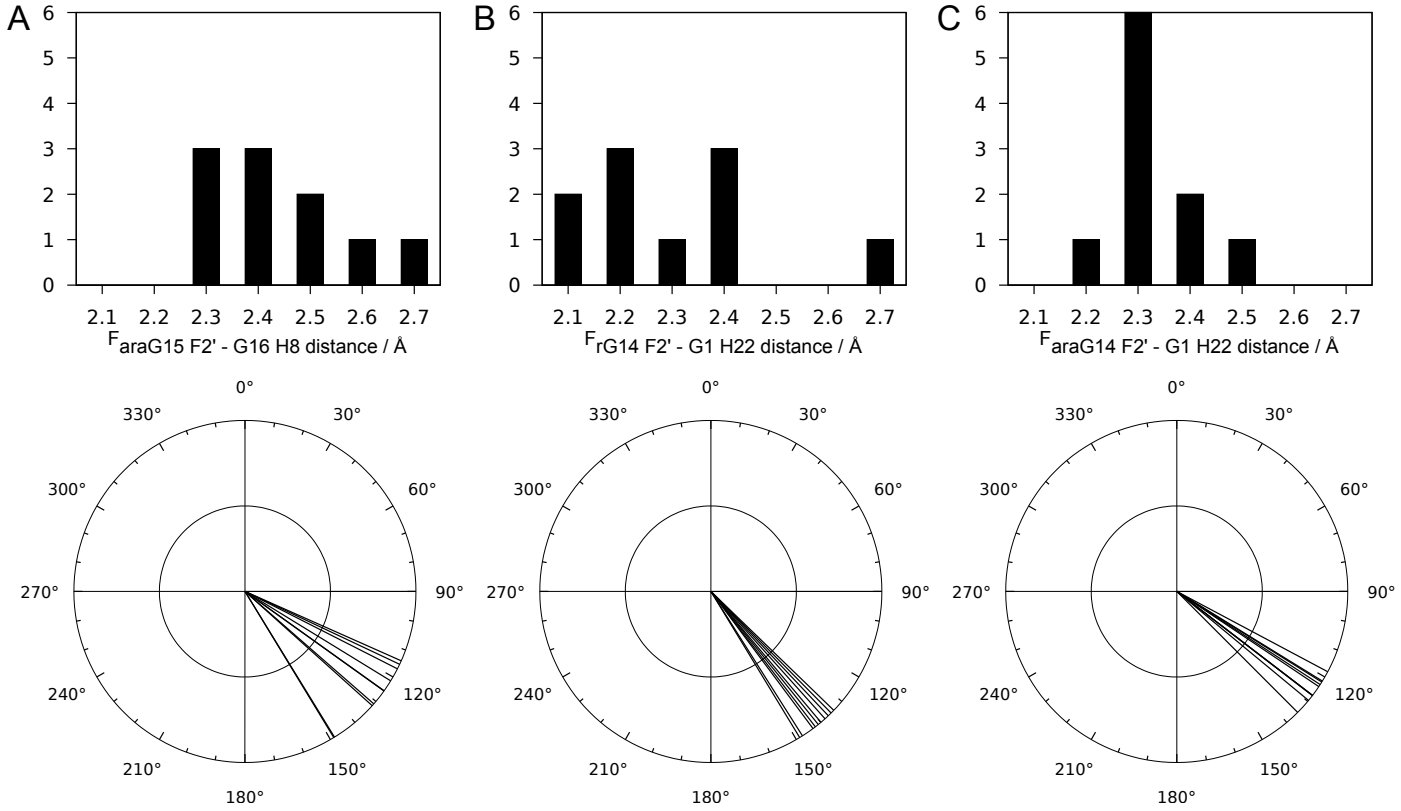

Fig. S16 Geometric parameters of the F· · ·H-C (A) and F· · ·H-N (B) hydrogen bond in F14A15 and of the F· · ·H-N hydrogen bond in A14F15 (C). Histograms in the top panel show the distribution of F-H distances in the ten structures of lowest energy and values of corresponding F-H-C or F-H-N angles are plotted in the bottom panel.

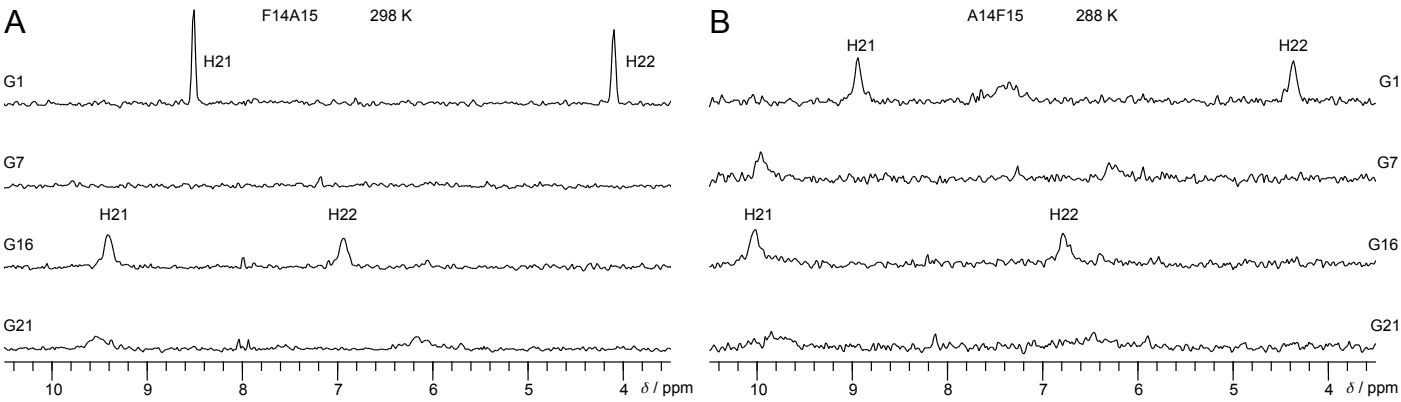

Fig. S17 2D NOE projections along ω_1 of intraresidual imino-amino correlations for central tetrad residues in F14A15 at 25 °C (A) and in A14F15 at 15 °C (B). Spectra were acquired with concentrations of 0.4 mM in 10 mM KP_i buffer, pH 7, with a mixing time of 300 ms. A) For G1, sharp amino resonances with linewidths of 25-30 Hz indicate hindrance of the amino group rotation through involvement of H21 and H22 amino protons in hydrogen bonding within the tetrad and with ^{F}rG14 F2', respectively. Other amino resonances of the central tetrad are considerably broadened. Slowly exchanging H21 and H22 amino resonances of G16 exhibit linewidths of about 60 Hz. Here, amino group rotation is likely hampered by interactions of G16 H22 with A18 N7 (Fig. S14). B) Whereas at 25 °C all central tetrad amino resonances of A14F15 are mostly broadened beyond detection (not shown), G1 H21 and H22 resonances are in slow exchange at 15 °C with linewidths of about 50 Hz and with chemical shifts similar to F14A15, again pointing to a G1 H22 ^{F}araG14 F2' interaction. As for F14A15, amino resonances of G16 are also in slow exchange, suggesting similar G16-A18 interactions.

Supplementary Tables

Tab. S1 UV melting temperatures T_m of A14F15 and F14A15 in low-salt and high-salt potassium buffer, pH 7.[a]

	10 mM KP_i		20 mM KP_i, 100 mM KCl	
	T_m / °C	standard deviation	T_m / °C	standard deviation
A14F15	37.7	0.8	55.8	0.4
F14A15	38.3	0.2	56.8	0.5

[a]measured in triplicate

Tab. S2 Experimentally determined ^{19}F-^{1}H scalar couplings of ^{F}araG and ^{F}rG residues of A14F15 and F14A15 measured from ^{1}H-^{1}H 2D NOE, DQF-COSY, or TOCSY crosspeaks at 25 °C (uncertainty ± 1 Hz).

	A14F15		F14A15	
	^{F}araG14	^{F}rG15	^{F}rG14	^{F}araG15
$^{2}J_{\mathrm{F2'H2'}}$	53.4 Hz	52.8 Hz	51.6 Hz	49.8 Hz
$^{3}J_{\mathrm{F2'H1'}}$	1.2 Hz	28.2 Hz	10.2 Hz	20.4 Hz
$^{3}J_{\mathrm{F2'H3'}}$	18.0 Hz	23.4 Hz	~ 0	~ 0
$^{h1}J_{\mathrm{F2'H8(n+1)}}$	-	-	-	1.2 Hz

Tab. S3 NMR restraints and structural statistics for the structure calculations of A14F15 and F14A15.

	A14F15	**F14A15**
NOE distance restraints		
intraresidual	71	77
sequential	54	69
long-range	23	43
other restraints		
hydrogen bonds	48	52
torsion angles	39	39
structural statistics		
pairwise heavy atom RMSD / Å		
G-core	0.68 ± 0.10	0.92 ± 0.24
all residues	3.94 ± 0.49	2.96 ± 0.65
violations / Å		
maximum NOE violation	0.16	0.13
mean NOE violation	0.003 ± 0.001	0.002 ± 0.001
deviations from idealized geometry		
bonds / Å	0.01 ± 0.00	0.01 ± 0.00
angles / degree	2.31 ± 0.03	2.28 ± 0.04

Tab. S4 Half-widths $\nu_{1/2}$ of the G1 H21 and G1 H22 resonances of F14A15 as determined from NOESY traces along ω_2 with and without ^{19}F decoupling.[a]

intraresidual 2D NOE crosspeak of G1	$\nu_{1/2}$ ^{19}F non-decoupled	$\nu_{1/2}$ ^{19}F decoupled	$\Delta\nu_{1/2}$
H1(ω_1) – H21 (ω_2)	19.1 Hz	19.3 Hz	0.2 Hz
H22(ω_1) – H21 (ω_2)	20.0 Hz	20.8 Hz	0.8 Hz
H1(ω_1) – H22 (ω_2)	25.0 Hz	21.1 Hz	-3.9 Hz
H21(ω_1) – H22 (ω_2)	23.6 Hz	18.7 Hz	-4.9 Hz

[a] uncertainty ± 1.2 Hz

Tab. S5 ^{1}H, ^{13}C, and ^{19}F chemical shifts of A14F15 at 25 °C in 10 mM KP_i, pH 7.[a]

δ / ppm	H8/H6	C8/C6	H1'	H2'/H2"	H3'	H4'	H1	H5/H2/Me/F2'
G1	7.24	140.6	5.75	2.35/2.66	4.90	n.d.	11.92	-
G2	7.52	137.4	5.83	2.39/2.56	4.97	n.d.	11.74	-
G3	7.94	139.4	5.81	2.55/2.49	4.83	n.d.	n.d.	-
A4	8.03	141.8	6.08	2.41/2.43	n.d.	n.d.	-	7.85
T5	7.28	139.2	5.89	1.93/2.32	4.64	n.d.	n.d.	1.56
G6	7.30	142.1	5.98	3.43/2.89	4.87	n.d.	11.65	-
G7	8.08	138.5	5.94	2.64/2.84	5.04	n.d.	12.01	-
G8	7.44	137.5	5.95	2.14/2.56	4.91	n.d.	11.34	-
A9	n.d.	n.d.	n.d.	n.d./n.d.	n.d.	n.d.	-	n.d.
C10	7.73	143.9	6.12	2.30/n.d.[b]	4.96	n.d.	-	6.06
A11	n.d.	n.d.	n.d.	n.d./n.d.	n.d.	n.d.	-	n.d.
C12	7.54	143.8	5.75	2.16/1.89	4.59	n.d.	-	5.75
A13	7.98	141.6	5.96	2.16/2.42[b]	n.d.	n.d.	-	n.d.
^{F}araG14	7.30	141.0	6.21	5.86/-	6.26	n.d.	10.79	-124.31
^{F}rG15	7.31	136.4	5.97	5.80/-	4.82	4.33	11.44	-117.05
G16	7.63	138.6	6.06	3.00/2.52	4.96	n.d.	11.69	-
G17	7.85	137.9	6.38	2.65/2.65	5.06	n.d.	11.12	-
A18	8.55	142.9	6.55	2.99/2.89	4.98	n.d.	-	n.d.
C19	7.95	145.3	6.40	2.50/2.66	4.95	n.d.	-	6.09
G20	7.38	142.1	6.01	3.08/3.03	4.93	n.d.	11.92	-
G21	8.18	139.0	6.06	2.82/2.86[b]	5.11	n.d.	11.72	-
G22	7.79	138.0	6.44	2.62/2.53	4.74	n.d.	11.41	-

[a] n.d. - not determined

[b] no stereospecific assignment

Tab. S6 ^{1}H, ^{13}C, and ^{19}F chemical shifts of F14A15 at 25 °C in 10 mM KP_i, pH 7.[a]

δ / ppm	H8/H6	C8/C6	H1'	H2'/H2"	H3'	H1	H5/H2/Me/F2'	amino
G1	7.18	139.7	6.01	2.61/2.88	4.94	11.43	-	8.51/4.10
G2	7.57	141.2	5.94	2.34/2.47[b]	4.98	11.19	-	n.d./n.d.
G3	7.80	139.5	5.41	2.25/2.35	4.58	n.d.	-	n.d./n.d.
A4	8.01	142.0	5.88	2.40/2.32	4.71	-	7.78	n.d./n.d.
T5	7.19	139.6	5.51	2.16/2.35	4.60	n.d.	1.41	-/-
G6	8.04	138.9	5.88	2.79/2.89	4.97	11.31	-	n.d./n.d.
G7	7.94	137.3	6.09	2.66/2.86	5.04	11.69	-	n.d./n.d.
G8	7.39	137.2	5.98	1.90/2.41	4.93	11.27	-	n.d./n.d.
A9	8.37	142.8	6.34	2.83/2.70	5.10	-	n.d.	n.d./n.d.
C10	7.49	143.3	5.84	2.11/1.64	n.d.	-	5.86	n.d./n.d.
A11	7.85	141.4	5.76	2.39/n.d.	4.62	-	n.d.	n.d./n.d.
C12	7.28	143.5	5.70	2.10/2.16	n.d.	-	5.50	n.d./n.d.
A13	7.80	140.9	5.94	2.04/2.96	4.87	-	7.74	8.12/3.96
^{F}rG14	6.82	141.7	5.70	6.30/-	4.97	10.79	-127.83	n.d./n.d.
^{F}araG15	7.85	138.0	6.26	5.41/-	4.70	11.89	-116.23	n.d./n.d.
G16	7.88	140.0	6.07	2.84/2.72[b]	5.06	11.57	-	9.40/6.94
G17	7.84	138.2	6.25	2.67/2.54	4.98	11.25	-	n.d./n.d.
A18	8.58	143.1	6.54	3.05/2.93	n.d.	-	8.36	n.d./n.d.
C19	7.95	145.0	6.38	2.44/2.66	n.d.	-	n.d.	n.d./n.d.
G20	7.88	138.5	6.07	2.39/2.86	4.78	11.52	-	n.d./n.d.
G21	8.00	138.1	6.19	2.86/2.91	5.08	11.48	-	n.d./n.d.
G22	7.78	137.9	6.42	2.64/2.50	4.74	11.39	-	n.d./n.d.

[a] n.d. - not determined

[b] no stereospecific assignment